KSTLE International Journal, Vol. 9, No. 1/2, December 2008, pp. 1-6

FE Lubrication Analysis and Dynamic Characteristics of Herringbone Groove Air Bearing applied to High-Speed Color Wheel

An Sung Lee†

System Engineering Research Division, Korea Institute of Machinery and Materials, Daejeon, Korea

Abstract: In this study is performed a complex lubrication analysis of a herringbone groove air journal bearing, which shows a big potential as an oilless bearing for a color wheel used as an original color source for a large DLP projection television and rotating at a rated-speed of 10,800 rpm. The Galerkin FE and perturbation methods are used for a lubrication analysis of the bearing. The effects of groove number, angle and depth and bearing clearance on the dynamic stability of the bearing are investigated in terms of the critical mass, and its equilibrium positions, stiffness and damping coefficients are calculated at various rotating speeds. Results have shown that the designed herringbone groove air journal bearing is quite suitable as a support bearing for the considered high-speed color wheel in terms of the complex lubrication performances of the bearing itself.

Keywords: *galerkin FE, lubrication analysis, dynamic stability, herringbone groove air bearing, color wheel*

1. Introduction

As the digital technology has advanced so rapidly, now is spotlighted a projection television of utilizing DLP (digital light processing) with a high resolution rather than CRT's (cathode-ray tubes) with a low resolution in the past. In the CRT television video signals of red, green and blue colors from three separate CRT's are projected and combined on the screen. But the DLP television has no CRT's. Instead, it has one high intensity lamp, projecting one image on the screen.

A heart of the DLP technology is a DMD (digital micro-mirror device). About 900,000 pieces of micro-mirrors act as on/off switches by utilizing static voltages upon receiving their individual signals and express 256 gray scales in an on/off time. At this time, a color wheel passes glasses coated with red, green and blue colors in turn and generates colors. As the process proceeds so rapidly, by cheating human eyes, the color wheel expresses a red color first, and then in turn a green and blue color, and a human does not sense much difference.

The color wheel maintains a precise rotating speed by receiving a signal from an exclusive motor drive chip. An existing color wheel operated at 9,000 rpm. But a state of the art leading color wheel is now improved to operate at 10,800 rpm and thereby a human does not sense any color separation much better. In this color wheel performances of its motor and bearing are very important. Its rotating speed must be kept constant, and at a low noise state without generating any annoying abnormal sound, it should have a capability of running over 50,000 hours without any mechanical failure. To serve these purposes, in a view point of mechanical engineering, need to be developed a complex lubrication design analysis technology of supporting bearing, providing a smooth rotation both at a start-up of low speed and at a rated normal state of high speed, and an accurate rotordynamic design analysis technology, keeping the vibration of a color wheel rotor at a possible minimum, which is felt as a noise by a customer.

Since herringbone groove journal bearings show significantly improved stability characteristics even at their journal concentric operation states in high-speeds, today they find

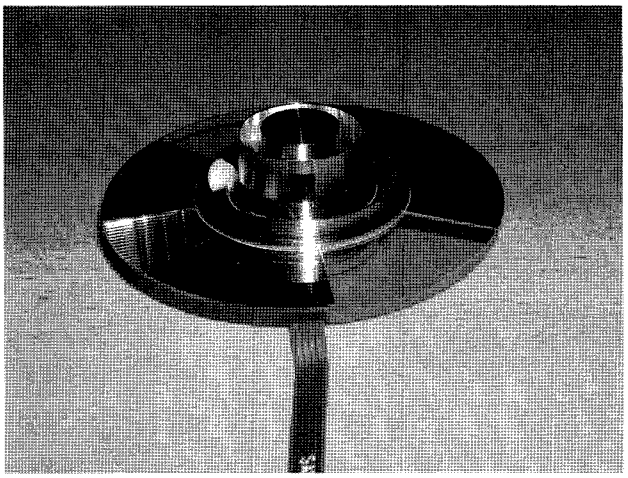

Fig. 1. Photo of color wheel assembly for a large DLP projection television.

†Corresponding author; aslee@kimm.re.kr
Tel: +82-42-868-7356, Fax : +82-42-868-7440

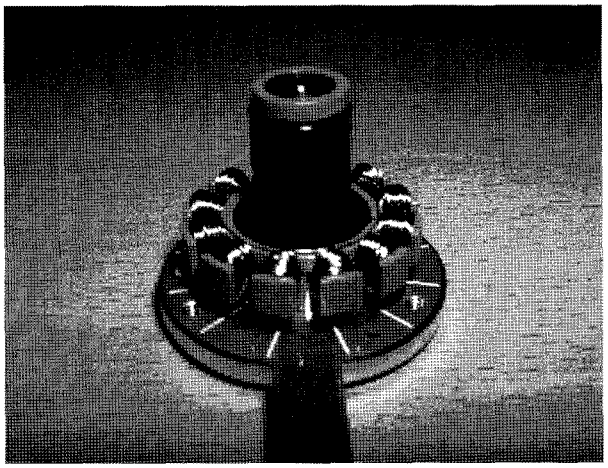

Fig. 2. Photo of herringbone grooved air journal bearing for a color wheel.

wide applications in high-speed lightweight machinery such as computer hard disk drives, polygon-mirror laser scanners found in laser printers, copiers, displays, laser plate making systems and high-speed facsimiles, and gyroscopes and dental tools, etc. [1-3].

In the past NGT (narrow groove theory, [4,5]), which assumed an infinite number of grooves, had been widely used in the hydrodynamic lubrication analyses of herringbone groove bearings. And NGT was reported to give some practical results for number of grooves with more than 16 [6]. But because of quite narrow machining spaces and especially to save machining expenses, herringbone groove journal bearings with small number of grooves are preferred in practical applications. In order to overcome the limits of NGT, in the present the finite difference method [7] and the finite element method [6] [8,9] are more widely used. On the other hand, high-speed gas bearings should sustain the dynamic stability, and often the critical mass is used in the stability analysis of bearing for a simple lumped-mass rotor [10].

Figure 1 shows the color wheel assembly used as an color source for a large DLP projection television. Figure 2 shows the herringbone groove air journal bearing which supports the color wheel rotor and it is observed that the herringbone grooves are engraved on the stationary journal shaft. In this study is performed a complex lubrication analysis of a herringbone groove air journal bearing, which shows a big potential as an oilless bearing for a color wheel and rotating at a rated-speed of 10,800 rpm. The Galerkin FE and perturbation methods are used for a lubrication analysis of the bearing. The effects of groove number, angle and depth and bearing clearance on the dynamic stability of the bearing are investigated in terms of the critical mass, and its equilibrium positions, stiffness and damping coefficients are calculated at various rotating speeds.

2. FE Lubrication Formulation and Solution Procedure

Figure 3 shows geometries of the herringbone groove air journal bearing along with its design parameters, and Figure 4 shows the bearing coordinate systems necessary for analyses. The nondimensionalized Reynolds equation for a herringbone groove air journal bearing is expressed by

$$\frac{\partial}{\partial Z}\left(PH^3\frac{\partial P}{\partial Z}\right)+\frac{\partial}{\partial\theta}\left(PH^3\frac{\partial P}{\partial\theta}\right)=\Lambda\frac{\partial}{\partial\theta}(PH)+j2\sigma\Lambda\frac{\partial}{\partial\tau}(PH) \tag{1}$$

where $H = 1+<H_\delta>+e\ cos(\theta-\phi)$. $<H_\delta>$ represents a groove depth and is considered only in a groove area. Introducing a complex notation and considering a small perturbation of the journal from its equilibrium position, the bearing film thickness and pressure can be expressed by

$$H = H_0+\Delta Xe^{\tau}\ cos\theta+\Delta Ye^{\tau}\ sin\theta \tag{2}$$

$$P = P_0+\Delta Xe^{\tau}P_1+\Delta Ye^{\tau}P_2 \tag{3}$$

where $P_1 = P_x+jP_{\dot{x}}$ and $P_2 = P_Y+jP_{\dot{Y}}$. Then, the perturbed Reynolds equations are given by

$$0:\ \frac{\partial}{\partial Z}\left(P_0H_0^3\frac{\partial P}{\partial Z}\right)+\frac{\partial}{\partial\theta}\left(P_0H_0^3\frac{\partial P}{\partial\theta}\right)=\Lambda\frac{\partial}{\partial\theta}(P_0H_o) \tag{4.a}$$

$$\begin{aligned}\Delta X:\ &\frac{\partial}{\partial Z}\left(H_0^3\frac{\partial P_0P_1}{\partial Z}+3P_0H_0^2cos\theta\frac{\partial P_0}{\partial Z}\right)\\&+\frac{\partial}{\partial\theta}\left(H_0^3\frac{\partial P_0P_1}{\partial\theta}+3P_0H_0^2cos\theta\frac{\partial P_0}{\partial\theta}\right)\\&=\Lambda\frac{\partial}{\partial\theta}(P_0cos\theta+P_1H_0)+j2\sigma\Lambda(P_0cos\theta+P_1H_0)\end{aligned} \tag{4.b}$$

$$\begin{aligned}\Delta Y:\ &\frac{\partial}{\partial Z}\left(H_0^3\frac{\partial P_0P_2}{\partial Z}+3P_0H_0^2sin\theta\frac{\partial P_0}{\partial Z}\right)\\&+\frac{\partial}{\partial\theta}\left(H_0^3\frac{\partial P_0P_2}{\partial\theta}+3P_0H_0^2sin\theta\frac{\partial P_0}{\partial\theta}\right)\\&=\Lambda\frac{\partial}{\partial\theta}(P_0sin\theta+P_2H_0)+j2\sigma\Lambda(P_0sin\theta+P_2H_0)\end{aligned} \tag{4.c}$$

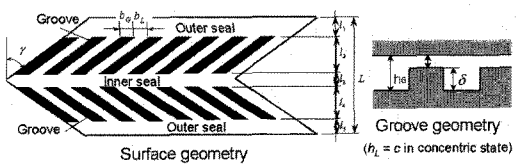

Fig. 3. Geometries and design parameters of a herringbone groove air journal bearing.

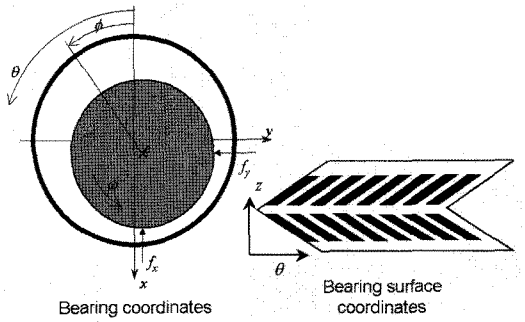

Fig. 4. Coordinate systems of a herringbone groove air journal bearing.

A Galerkin FE formulation of the Reynolds equation is carried out by applying a weighted residual integral to each perturbed equation of Eq. (4) for each individual element and expanding it through integration by parts. Finally, the FE equations of the perturbed Reynolds equations are given by the following matrix form:

$$[k^e]\{P^e\} = \{r^e\} \tag{5}$$

Where

$$0:\ K_{ij}^e = \iint_e \begin{bmatrix} P_0 H_0^3\left(\frac{\partial N_i}{\partial Z}\frac{\partial N_j}{\partial Z} + \frac{\partial N_i}{\partial \theta}\frac{\partial N_j}{\partial \theta}\right) \\ -\Lambda H_0 \frac{\partial N_i}{\partial \theta} N_j \end{bmatrix} dA$$

$$P^e = P_{0j}^e \tag{5.a}$$

$$r_i^e = B\ .L.I.\ terms$$

$$\Delta X:\ K_{ij}^e = \iint_e \begin{bmatrix} P_0 H_0^3\left(\frac{\partial N_i}{\partial Z}\frac{\partial N_j}{\partial Z} + \frac{\partial N_i}{\partial \theta}\frac{\partial N_j}{\partial \theta}\right) \\ + H_0^3\left(\frac{\partial N_i}{\partial Z}\frac{\partial P_0}{\partial Z} + \frac{\partial N_i}{\partial \theta}\frac{\partial P_0}{\partial \theta}\right) N_j \\ -\Lambda H_0 \frac{\partial N_i}{\partial \theta} N_j + j2\sigma\Lambda H_0 N_i N_j \end{bmatrix} dA \tag{5.b}$$

$$P^e = P_{1j}^e$$

$$r_i^e = -\iint_e \begin{bmatrix} 3P_o H_0^2\left(\frac{\partial N_i}{\partial Z}\frac{\partial P_0}{\partial Z} + \frac{\partial N_i}{\partial \theta}\frac{\partial P_0}{\partial \theta}\right) \\ -\Lambda P_0 \frac{\partial N_i}{\partial \theta} + j2\sigma\Lambda P_0 N_i \end{bmatrix} \cos\theta dA$$

$$+ B.L.I.\ terms$$

$$\Delta Y:\ k_{ij}^e = \iint_e \begin{bmatrix} P_0 H_0^3\left(\frac{\partial N_i}{\partial Z}\frac{\partial N_j}{\partial Z} + \frac{\partial N_i}{\partial \theta}\frac{\partial N_j}{\partial \theta}\right) \\ + H_0^3\left(\frac{\partial N_i}{\partial Z}\frac{\partial P_0}{\partial Z} + \frac{\partial N_i}{\partial \theta}\frac{\partial P_0}{\partial \theta}\right) N_j \\ -\Lambda H_0 \frac{\partial N_i}{\partial \theta} N_j + j2\sigma\Lambda H_0 N_i N_j \end{bmatrix} dA \tag{5.c}$$

$$P^e = P_{2j}^e$$

$$r_i^e = -\iint_e \begin{bmatrix} 3P_0 H_0^2\left(\frac{\partial N_i}{\partial Z}\frac{\partial P_0}{\partial Z} + \frac{\partial N_i}{\partial \theta}\frac{\partial P_0}{\partial \theta}\right) \\ -\Lambda P_0 \frac{\partial N_i}{\partial \theta} + j2\sigma\Lambda P_0 N_i \end{bmatrix} \sin\theta\ dA$$

$$+ B.L.I.\ terms$$

The assembled equations of Eq. (5) for the entire elements are solved, applying the boundary conditions and utilizing the Newton-Raphson method. Then, the load carrying capacities, stiffness and damping coefficients of the bearing are obtained by

$$F_X = \frac{f_x}{P_a R^2} = \iint_A P_0 \cos\theta dZ d\theta \tag{6.a}$$

$$F_Y = \frac{f_y}{P_a R^2} = \iint_A P_0 \sin\theta dZ d\theta$$

$$\begin{bmatrix} K_{XX} & K_{XY} \\ K_{YX} & K_{YY} \end{bmatrix} = \frac{c}{P_a R^2}\begin{bmatrix} k_{xx} & k_{xy} \\ k_{yx} & k_{yy} \end{bmatrix} \tag{6.b}$$

$$= \iint_A Re\begin{bmatrix} P_1\cos\theta & P_2\cos\theta \\ P_1\sin\theta & P_2\sin\theta \end{bmatrix} dZ d\theta$$

$$\begin{bmatrix} C_{XX} & C_{XY} \\ C_{YX} & C_{YY} \end{bmatrix} = \frac{cv}{P_a R^2}\begin{bmatrix} c_{xx}^* & c_{xy}^* \\ c_{yx}^* & c_{yy}^* \end{bmatrix} \tag{6.c}$$

$$= \iint_A \mathrm{Im}\begin{bmatrix} P_1\cos\theta & P_2\cos\theta \\ P_1\sin\theta & P_2\sin\theta \end{bmatrix} dZ d\theta$$

Besides, an equilibrium journal position, (e_0, ϕ_0), at the force equilibrium between the bearing force and the journal weight or any given external force can be calculated, utilizing the Newton-Raphson method.

Assuming the journal as a rigid body having only translational degrees of freedom, its nondimensionalized homogenous equation of motion is expressed by

$$\begin{aligned} -\sigma^2 M\frac{d^2X}{d\tau^2} + jC_{XX}\frac{dX}{d\tau} + jC_{XY}\frac{dY}{d\tau} + K_{XX}X + K_{XY}Y = 0 \\ -\sigma^2 M\frac{d^2Y}{d\tau^2} + jC_{YX}\frac{dX}{d\tau} + jC_{YY}\frac{dY}{d\tau} + K_{YX}X + K_{YY}Y = 0 \end{aligned} \tag{7}$$

where $M = mc\omega^2/(p_a R^2)$. Substituting $X = X_0 e^{\tau}$ and into Eq. (7) and arranging it in a matrix form,

$$\begin{bmatrix} -\sigma^2 M + K_{XX} + jC_{XX} & jC_{XY} + K_{XY} \\ jC_{YX} + K_{YX} & -\sigma^2 M + K_{YY} + jC_{YY} \end{bmatrix}\begin{Bmatrix} X_0 \\ Y_0 \end{Bmatrix} = \begin{Bmatrix} 0 \\ 0 \end{Bmatrix} \tag{8}$$

For a nontrivial solution of Eq. (8), its determinant should be 0.

$$\begin{aligned} \det = \{(-\sigma^2 M + K_{XX})(-\sigma^2 M + K_{YY}) - C_{XX}C_{YY}\} \\ + C_{XY}C_{YX} - K_{XY}K_{YX}\} + j\{C_{XX}(-\sigma^2 M + K_{YY})\} \\ + C_{YY}(-\sigma^2 M + K_{XX}) - C_{XY}K_{YX} - C_{YX}K_{XY}\} = 0 \end{aligned} \tag{9}$$

Therefore, both the real and imaginary parts of Eq. (9) should be.

$$\mathrm{Re(det)}{=}0: \quad \begin{aligned} &(-\sigma^2 M + K_{XX})(-\sigma^2 M + K_{YY}) \\ &- C_{XX}C_{YY} + C_{XY}C_{YX} - K_{XY}K_{YX} = 0 \end{aligned} \tag{10.a}$$

$$\mathrm{Im(det)}{=}0:$$

$$M = \frac{C_{YY}K_{XX} + C_{XX}K_{YY} - C_{XY}K_{YX} - C_{YX}X_{XY}}{\sigma^2(C_{XX} + C_{YY})} \tag{10.b}$$

Then, a threshold whirl frequency ratio at which the journal motion becomes unstable is calculated from Eq. (10.a) by utilizing the Newton-Raphson method and its associated critical mass of instability is calculated from Eq. (10.b).

3. Results and Discussions

A complex lubrication analysis of a herringbone groove air

Table 1. Basic design parameters and operating condifition of the herringbone groove bearing.

Groove number, N_G	9
Bearing radius, R, (mm)	4
Groove angle, γ, (deg.)	30
Groove depth, δ, (μm)	3
Bearing clearance, c,(μm)	4
Groove width ratio, b_G:b_L	05 : 0.5
Journal mass, m, (g)	16.8
Rated operating speed, ω, (rpm)	10,800
Air viscosity, μ, (Pa · s)	1.87e-05

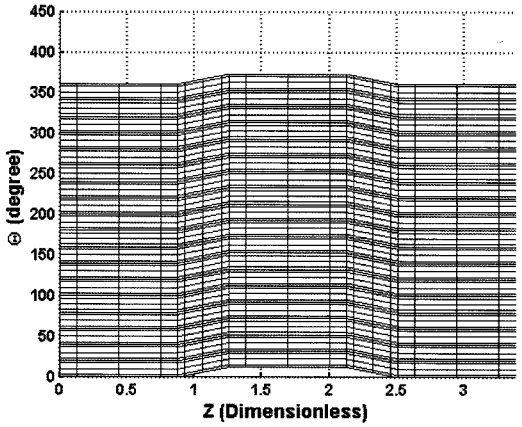

Fig. 5. FE mesh of the bearing for γ=30°.

journal bearing, which shows a big potential as an oilless bearing for a color wheel used as an original color source for a large DLP projection television, was performed. The basic design parameters and operating conditions of the bearing are given in Table 1, and Figure 5 shows the FE mesh of the bearing for γ=30°. Figures. 6 and 7 show the pressure distribution generated at ω=10,800 rpm and its contour plot, respectively.

Figure 8 shows the critical mass characteristic of the bearing vs. a groove number, N_G, and it is noticed that as the groove

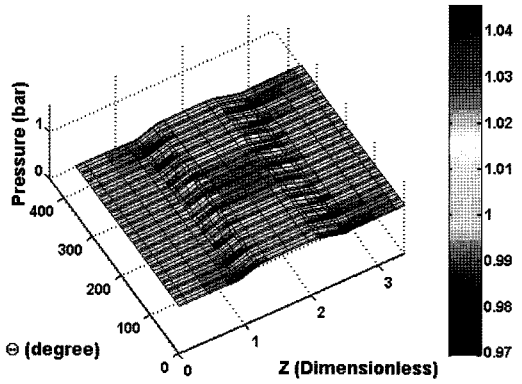

Fig. 6. Pressure distribution generated at ω = 10.800 rpm.

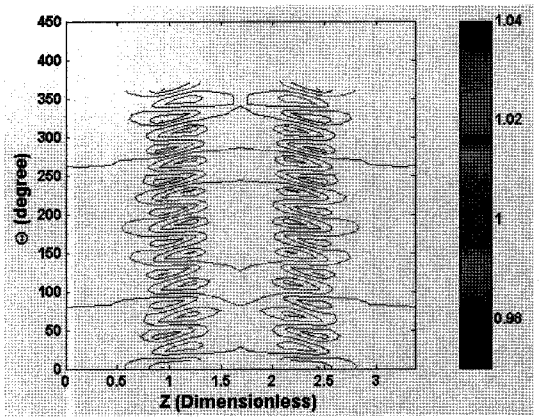

Fig. 7. Pressure contour obtained at ω = 10.80 rpm.

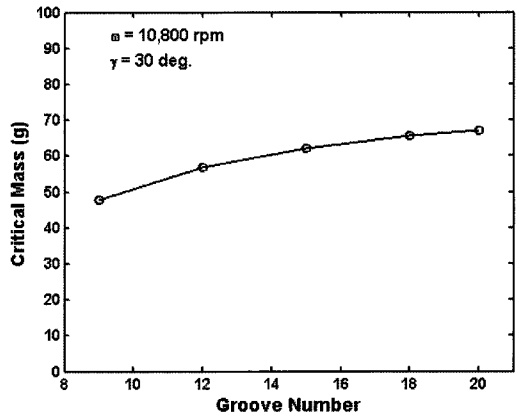

Fig. 8. Critical mass vs. groove number obtained at rpm and for .

number increases the critical mass, in other words, the stability increases. But upon considering the narrow machining space, machining cost and the rotor mass of 16.8 g, N_G=9 was selected for the bearing design. Figure 9 shows the critical mass characteristic of the bearing vs. a groove depth, δ, and it is noticed that the critical mass has the maximum value at around δ=3 μm.

Figure 10 shows the critical mass characteristic of the bearing

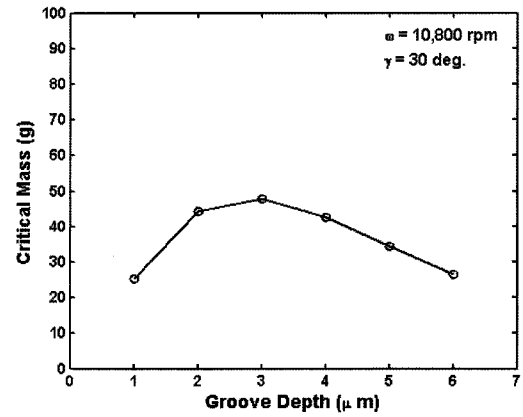

Fig. 9. Critical mass vs. groove depth obtained at rpm and for .

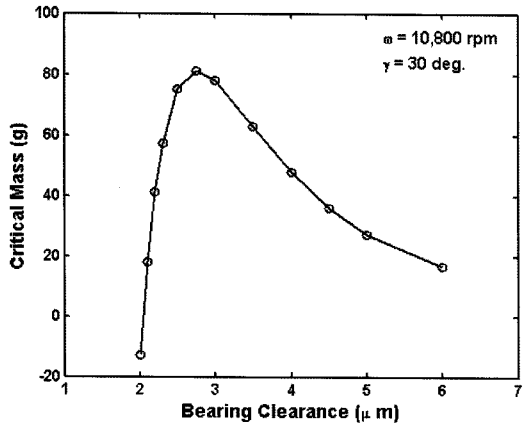

Fig. 10. Critical mass vs. bearing clearance obtained at ω=10,800 rpm and for γ=30°.

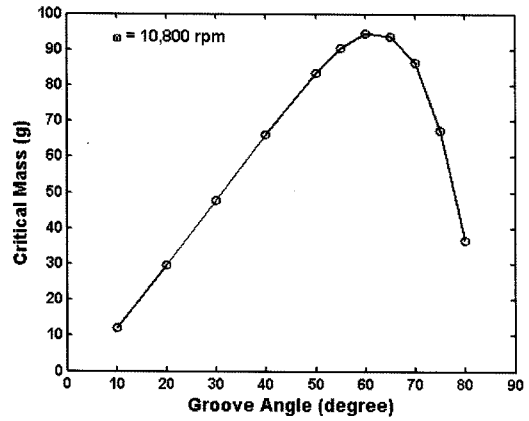

Fig. 11. Critical mass vs. groove angle obtained at ω=10,800 rpm.

vs. a bearing clearance, c , at rpm ω= 10.800 rpm and γ= 30°, and it is noticed that the critical mass has the maximum value at around $c = 3$ μm. Figure 11 shows the critical mass characteristic of the bearing vs. a groove angle, γ, at ω= 10.800 rpm, and it is noticed that the critical mass has the maximum value at around γ= 60°.

Figure 12 shows the critical mass characteristic of the bearing over a range of operating speeds for γ=30° and 60°. It is observed from the figure that as the operating speed increases the critical mass decreases sharply up to 4,000 rpm and thereafter decreases and converges slowly. Further, in terms of the critical mass γ=60° is somewhat more advantageous than 30°. Figure 13 shows the locus of the journal center (or the equilibrium position of the journal) at γ=30°.

It is noticed from the figure that the journal lifts off at about 100 rpm and that the journal runs nearly in a concentric state with little eccentricity at the rated speed of 10,800 rpm.

Figures. 14 and 15 show the bearing stiffness and damping coefficients over a range of operating speeds at γ=30°. Because of the unique characteristics of the herringbone groove bearing, it is observed as expected that the direct stiffness coefficients (*Kxx* and *Kyy*) and the direct damping coefficients (*Dxx* and *Dyy*) have nearly identical values from

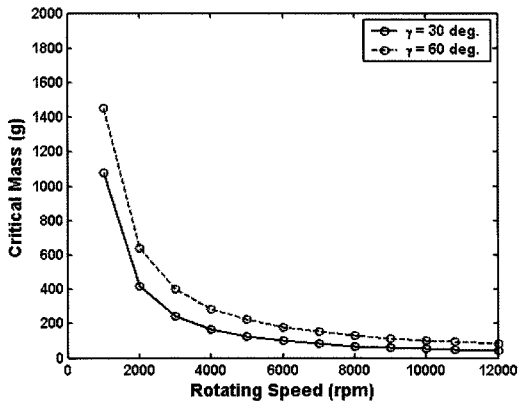

Fig. 12. Critical mass over a range of operating speeds for γ=30° and 60°.

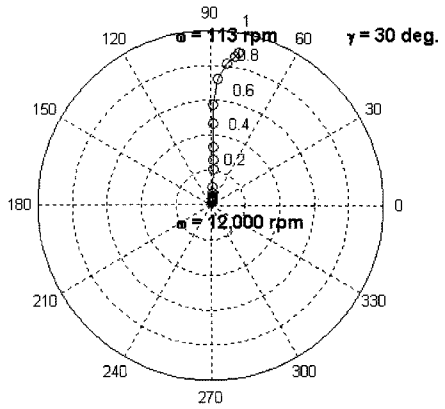

Fig. 13. Locus of the journal center over a range of operating speeds for γ=30° .

each other. Further, as the operating speed increases, the direct stiffness coefficients increase but the direct damping coefficients decrease.

4. Conclusions

In this study was performed a complex FE lubrication analysis of a herringbone groove air journal bearing, which shows a big potential as an oilless bearing for a color wheel used as an original color source for a large DLP projection television and rotating at a rated-speed of 10,800 rpm. The Galerkin FE and perturbation methods were used for a lubrication analysis of the bearing. The effects of groove number, angle and depth and bearing clearance on the dynamic stability of the bearing were investigated in terms of the critical mass, and its equilibrium positions, stiffness and damping coefficients were calculated at various rotating speeds. Results showed that the designed herringbone groove air journal bearing is quite suitable as a support bearing for the considered high-speed color wheel in terms of the complex lubrication performances of the bearing itself. As a future work, it will be required to analyze the complex rototordynamic characteristics, such as the critical speed and mode shape, stability and unbalance response, of the color wheel rotor

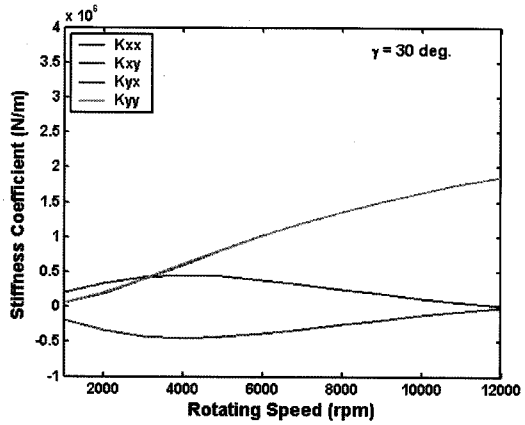

Fig. 14. Bearing stiffness coefficients over a range of operating speeds.

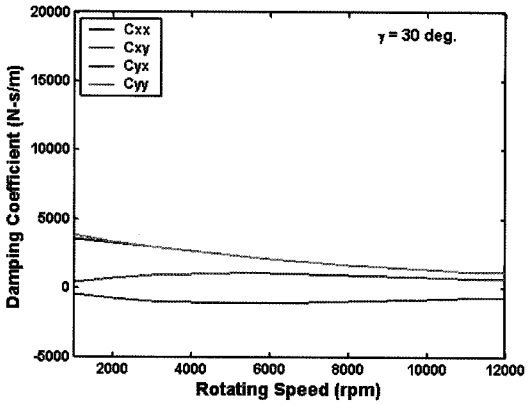

Fig. 15. Bearing damping coefficients over a range of operating speeds.

system supported on the herringbone groove air journal bearing.

Nomenclature

b_G, b_L	widths of groove and land
c	bearing radial clearance
c^*	damping coefficient
C	dimensionless damping coefficient, $cv/(P_a R^2)C^*$
e	eccentricity of journal
h	air film thickness
H	dimensionless air film thickness, h/c
j	$\sqrt{-1}$
k	stiffness coefficient
K	dimensionless stiffness coefficient, $cv/(P_a R^2)k$
l_1, l_2, l_3, l_4, l_5	lengths of outer seals, grooves and inner seal
L	bearing length
m	bearing support mass
M	dimensionless bearing support mass, $mc\omega^2/(p_a R^2)$
N_G	number of groove
P	pressure
P	dimensionless pressure, p/p_a
R	bearing or journal radius
x,y	x and y coordinates
X,Y	dimensionless x and y coordinates, x/c and y/c
z	axial coordinate of bearing
Z	dimensionless axial coordinate of bearing, z/R
δ	groove depth, h_G-h_L
ϕ	attitude angle of journal
γ	groove angle
μ	viscosity of air
ν	whirl exciting frequency
θ	angular coordinate of bearing
σ	whirl frequency ratio, ν/ω
τ	dimensionless time, $j\ vt$
ω	rotating speed

Subscripts

α	ambient
G	groove
L	land
0	equilibrium or initial state

References

1. Tanaka, K., and Muraki, H., "Performance of Air-Lubricated Hydrodynamic Bearing Spindles for Laser Scanners," ASME Journal of Tribology, Vol. 113, pp. 609-614, 1991.
2. Zhang, Q. D., Chen, S. X., and Liu, Z. J., "Design of A Hybrid Fluid Bearing System for HDD Spindles," IEEE Transactions on Magnetics, Vol. 35(2), pp. 821-826, 1999.
3. Lee, Y.-Z., Jeong, S.-H., and Jeong, K.-S., "Frictional and Electrical Characteristics of Grooved Fluid Film Bearings for High-Speed Laser Scanner Motor," ASME Journal of Tribology, Vol. 122, pp. 557-564, 2000.
4. Vohr, J. H., and Chow, C. Y., "Characteristics of Herringbone-Grooved Gas-Lubricated Journal Bearings," ASME Journal of Basic Engineering, pp. 568-578, 1965.
5. Chow, C. Y., and Vohr., J. H., "Helical-Grooved Journal Bearing Operated in Turbulent Regime," ASME Journal of Lubrication Technology, pp. 346-358, 1969.
6. Bonneau, D., and Absi, J., "Analysis of Aerodynamic Journal Bearings with Small Number of Herringbone Grooves by Finite Element Methods," ASME Journal of Tribology, Vol. 116, pp. 698-704, 1994.
7. Kang, K., Rhim, Y., and Sung. K., "A Study of the Oil-Lubricated Herringbone-Grooved Journal Bearing-Part 1: Numerical Analysis," ASME Journal of Tribology, Vol. 118, pp. 906-911, 1996.
8. Zirkelback, N., and Luis, S. A, "Finite Element Analysis of Herringbone Groove Journal Bearings: A Parametric Study," ASME Journal of Tribology, Vol. 120, pp. 234-240, 1998.
9. Jang, G. H., and Kim, Y. J., "Calculation of Dynamic Coefficients in a Hydrodynamic Bearing Considering Five Degrees of Freedom for a General Rotor-Bearing System," ASME Journal of Tribology, Vol. 121, pp. 499-505, 1999.
10. Constantinescu, V. N., and Galetuse, S., "On the Dynamic Stability of the Spiral-Grooved Gas-Lubricated Thrust Bearing," ASME Journal of Tribology, Vol. 109, pp. 183-188, 1987.